Construction of amorphous structure models via relaxation of random arrangements of molecules

Jarod Worden,* Eric Cockayne, and Kevin F. Garrity
Material Measurement Laboratory, National Institute of Standards and Technology, Gaithersburg, Maryland 20899, USA

(Received 22 July 2025; revised 11 March 2026; accepted 23 June 2026; published 9 July 2026)

Amorphous materials have long been used in various technological applications, including semiconductor-based electronics. However, modeling amorphous materials at an atomic scale remains challenging. The melt-quench method is commonly used to generate models of amorphous structures, but the necessary lengthy molecular-dynamics runs can make calculations prohibitively expensive, especially for *ab initio* molecular dynamics. Furthermore, the relevance of melt-quench to athermal techniques like low-temperature deposition is unclear. We present an alternative method for constructing amorphous structures that starts with randomly placing molecules in a large box, followed by relaxation of the cell and atomic positions. We apply this approach to a variety of amorphous systems, using *ab initio* density-functional theory for the energetics, and obtain good agreement with experimental densities and radial distribution functions with less computational cost than the melt-quench method.

DOI: 10.1103/8cdr-bk3f

I. INTRODUCTION

Amorphous materials have long been utilized in technological applications including transistors, solar cells, thin-film devices, displays, flexible electronics, etc. [1–3]. Reasons for their widespread use include ease of fabrication, low-cost production, isotropic nature, and large area applications [3,4]. In semiconductor gate stacks, the lack of crystalline grain boundaries provides an advantage over crystalline oxides by reducing the potential paths for electrical breakdown [5]. Because amorphous materials are so prevalent, understanding their atomic structure through theoretical and simulation techniques is important for controlling their structural, electronic, and thermal characteristics. Unfortunately, compared with their crystalline counterparts, modeling amorphous structures is notoriously challenging. Amorphous structures lack long-range order but have important short-range order [6], necessitating a way to generate large unit cells that are random on long scales but capture the short-range atomic correlations seen in experiments.

The most common method of computationally constructing amorphous structures is the melt-quench technique, which uses molecular dynamics (MD) to mimic the experimental melt-quench technique [6–22]. *Ab initio* MD, which uses an *ab initio* method such as density-functional theory (DFT) to calculate forces and stresses, is typically the most accurate way to compute MD trajectories. However, DFT is also computationally costly, which can limit its application to unrealistically small unit cells and unphysically high quench rates.

To model larger systems and timescales, MD simulations utilizing interatomic potentials can reduce the computation time. However, producing and utilizing sufficiently accurate classical force fields is challenging [23]. Typically, there are a large number of parameters describing the atomic interactions that need to be fit to a large swath of theoretical and perhaps experimental data. [24–26]. Machine-learning force fields (MLFF) have steadily become one of the key methods for obtaining potentials that can produce near-DFT level results while reducing computational costs, allowing scalability for larger systems. The accuracy of MLFF for a given task depends on the availability of relevant data with which to train the models. While large databases exist for periodic materials, MLFF based on these data may not be transferable to the range of atomic environments characteristic of amorphous structures. Obtaining relevant data on amorphous structures to train future MLFF will require efficient methods using *ab initio* techniques [6].

In addition to the issue of accuracy versus speed that arises in MD melt-quench simulations of amorphous materials, it is worth noting that in many cases amorphous materials (such as amorphous semiconductors [27,28] and amorphous gate dielectrics [29]) are not experimentally produced by melt-quench techniques. This could potentially lead to inconsistencies between melt-quench-produced model structures and experimental data [4,6].

In this work, we present the molecule relaxation for amorphous structures (MRAS) method as a simple technique for efficiently constructing amorphous crystal structures using *ab initio* calculations and structure optimization alone, without the need for melt-quench MD. Our method starts by breaking a system into random moleculelike units that inherently contain partial local structure information, and then minimizing the total energy with respect to atomic positions and lattice parameters. We find that this method is capable of producing reasonable amorphous structures with less computational cost than the melt-quench method. We verify the accuracy of the method by comparing to experimental data on semiconducting, insulating, and metallic systems.

II. METHODOLOGY

Our basic procedure for generating amorphous structures, as summarized in Fig. 1, consists of randomly populating a

*Contact author: jarod.worden@nist.gov

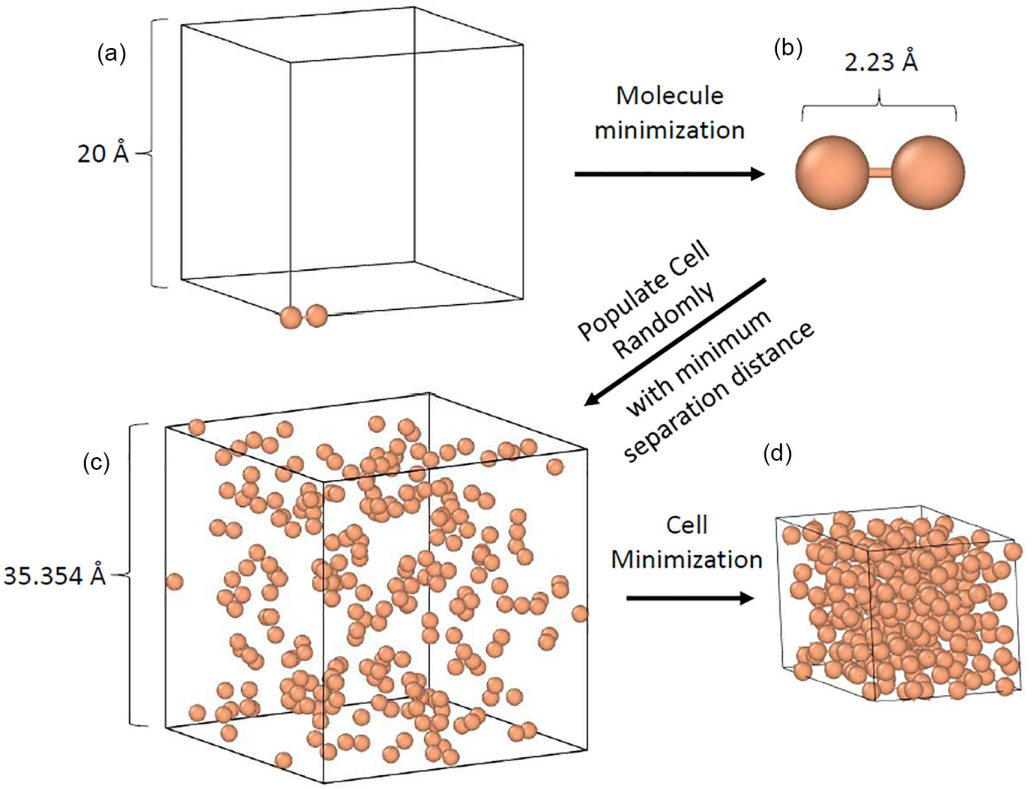

FIG. 1. Steps for creating amorphous structure are displayed in this workflow diagram. First, break down the desired amorphous compound into molecules of the appropriate composition [in this example, Si_2 for a-Si as shown in (a)] and relax an individual molecule to obtain its minimum energy configuration (b). Then, populate a large cell with replicas of this molecule using a minimum separation distance constraint (c). Finally, optimize the structure with respect to atomic position and cell shape to form the amorphous structure (d).

large unit cell with appropriate molecules that have a minimum separation distance between them and then performing structural optimizations. As an example, for Si, we start with a Si_2 dimer. The first step is to optimize the structure of the isolated molecule. This representative molecule is then used to populate a large, cubic simulation box along with random positions and orientations with a minimum separation distance between the molecules [30]. The procedure is conducted through an in-house code that takes initial values of cell parameters, molecule geometry, and minimum separation distance between molecules with periodic boundary conditions. Finally, the simulation cell is minimized with respect to atomic positions and cell lattice parameters. We apply the method in this work using density-functional theory to calculate the energy, forces, and stresses.

The reason we begin our method with molecules rather than single atoms is to avoid the system getting trapped with large composition gradients due to the randomness of the starting configuration. For example, an initial structure for SiO_2 based on random atomic positions will likely have initial regions that are randomly Si rich and O rich, in which atoms will have difficulty finding neighbors of the opposite type, potentially leading to unphysical clustering of elements in the relaxed structure. In particular, we found that O_2 molecules tended to form upon relaxation of initial random "monatomic" SiO_2 configurations (see also Ref. [31]). The molecular approach avoids this problem.

Our case studies in this paper are amorphous Si, SiO_2, HfO_2, ZrCu, and Al_2O_3. In the case of a-SiO_2 modeling, we initialize a random arrangement of linear SiO_2 molecules [32]. For HfO_2, we use a bent 3-atom HfO_2 molecule as this is found to be the lowest energy configuration [33]. For Al_2O_3, the formula unit suggests using a 5-atom molecule, but there are multiple choices for the Al_2O_3 molecule [34] and tests on the two lowest-energy 5-atom molecules yielded poor agreement with experiment, so we choose instead an equal mixture of 2-atom AlO and 3-atom AlO_2 molecules. As Si is monatomic, the argument for using a molecule rather than atomistic starting point is less compelling, but the 2-atom Si_2 molecule [35] was chosen for consistency with the binary examples.

A. Computational details

While the MRAS technique can be applied to any first-principles or molecular-dynamics code, in this work, we employ density-functional theory (DFT) using VASP [36–40]. The electronic structure calculations use a plane-wave basis set and projector augmented wave pseudopotentials [41,42], with the exchange and correlation potential approximated via the Perdew-Burke-Ernzerhof generalized gradient approximation functional [43]. To increase the speed of relaxation, the relaxation is performed in two successive conjugate gradient optimization stages. The first stage, for the larger initial

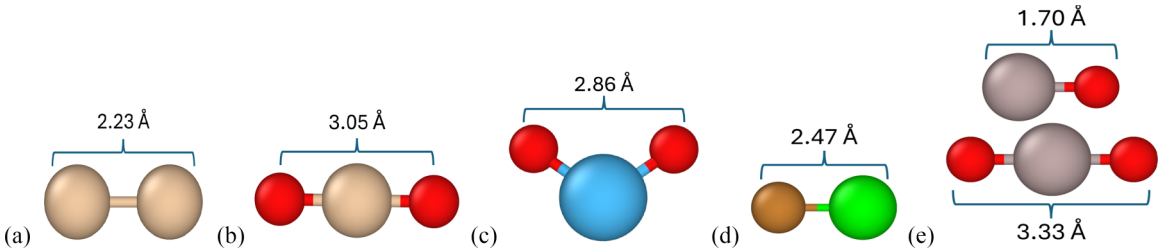

FIG. 2. Minimized molecule configurations for Si (a), SiO_2 (b), HfO_2 (c), ZrCu (d), and AlO and AlO_2 (e). The molecule lengths as displayed are the relaxed values. The HfO_2 molecule length (c) is represented by the second-nearest-neighbor distance when determining the separation distance for trimers when the minimum energy structure of the molecule is bent.

volume, uses the plane-wave cutoff energy of the largest minimum cutoff energy among the pseudopotentials of the individual elements and a k-point mesh of $1 \times 1 \times 1$. Once this stage is completed, the second relaxation stage uses a higher-energy cutoff of 500 eV and a k-point mesh of $2 \times 2 \times 2$. Relaxation with these parameters is repeated until the cell shape and energy converge.

Individual molecules for the case studies in this work are optimized by placing the dimer or trimer in a box with dimensions 20 Å × 20 Å × 20 Å to limit interactions of the molecule with its periodic images. A k-point mesh of $1 \times 1 \times 1$ with an energy cutoff of 500 eV is used with the conjugate gradient optimization and static box dimensions for relaxation. Trimers are initialized with a 135° bend, allowing the molecule to straighten or bend further. Indeed, the minimum energy configuration for HfO_2 is found to possess a bend, as can be seen in Fig. 2(c). Examples of relaxed molecule geometries are displayed in Fig. 2.

In this work, we also compare the MRAS method for Si, HfO_2, and ZrCu with the melt-quench method [44] as follows. For Si, we begin with a 216-atom crystalline cubic supercell, which is $3 \times 3 \times 3$ the conventional cell, i.e., with fixed dimensions of 16.41 Å× 16.41 Å× 16.41 Å [44,45]. The HfO_2 system is based off the monoclinic crystal structure with 96 atoms, which is $2 \times 2 \times 2$ the primitive cell, and the ZrCu one is based off the cubic crystal structure with 128 atoms, which is $4 \times 4 \times 4$ the primitive cell. These simulation cells were then scaled to match the densities of the amorphous structures found in literature [44–49]. The MD simulations utilize the Nosé-Hoover thermostat with a time step of 2 femtoseconds along with a k-point mesh of $1 \times 1 \times 1$ and an energy cutoff of 500 eV. Different conditions are investigated with respect to melt-time length, quench rate, and the final temperature, as melt-quench can be sensitive to these conditions. The initial melt temperature is 1.5× the melting temperature of the system (2500 K for Si, 4500 K for HfO_2, and 2500 K for ZrCu) with either 5- or 10-ps melt time [50–52]. After the melt, the temperature is quenched at a linear rate either for 10 or 20 ps with a target final temperature of 40 or 300 K. After the quench, a final hold of 5 ps at the target temperature is maintained.

III. RESULTS

We begin by testing various parameters for MRAS to find simulation conditions that lead to amorphous structures with properties close to experiment. In particular, we varied both the initial volume and the minimum separation distance between molecules. Silicon is used as the test material, with an initial cubic volume set to 3×, 5×, 7×, and 9× the expected volume. We independently vary the initial separation distance to 1.0×, 1.5×, and 2.0× the relaxed molecule length.

Due to the dependence of the final relaxed structures on the initial condition of randomly placed molecules, we use an ensemble of initial random configurations and compare the ensemble average properties of the relaxations for comparison with experimental data. A physical justification for this approach is to associate this ensemble averaging with spatial averaging—experimental amorphous materials have varying local densities within their global density [53].

We relax 20 different systems of 120 atoms for each combination of varying volume and separation distance. Figure 3 shows the final densities for varying volume and initial separation distance using this method. Increasing the initial volume decreases the final density, while increasing separation distance increases the final density. Note that increasing the separation distance (for the same volume and number of molecules) tends to make the initial distribution more spatially homogeneous up to the point where the effective packing fraction is too high to fit all the molecules.

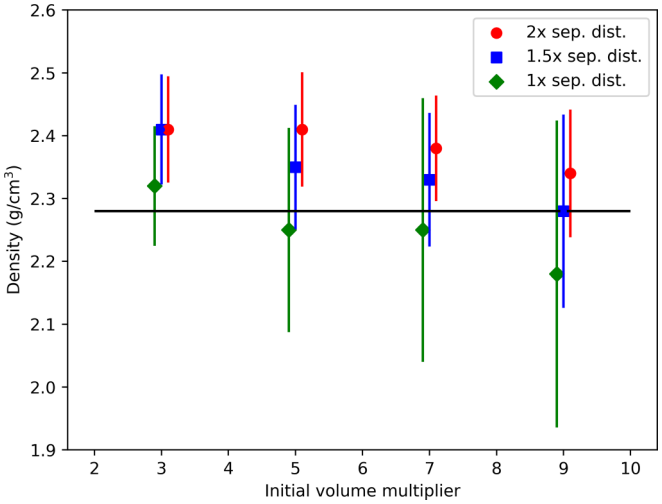

FIG. 3. Final densities of amorphous Si structures utilizing MRAS with varying the initial volume represented by the x-axis multiplier and varying separation distance (sep. dist.) with error bars representing 95% confidence level. The horizontal black line represents the experimental value for amorphous Si [44,45].

TABLE I. Initial minimum molecule separation distances for the amorphous systems investigated in this work.

Material	Si_2	SiO_2	HfO_2	ZrCu	Al_2O_3
Separation distance	3.34 Å	4.58 Å	4.29 Å	3.71 Å	3.72 Å

Based on the examples of Si and SiO_2, we use 9.0× the expected crystal volume and 1.5× separation distance of the molecule length for the rest of our simulations, except for the trimer/dimer combination of Al_2O_3, where we use a separation distance that is 1.5× the length of the average length of the molecules. The separation distances used are displayed in Table I.

Using our established choices for the initial volume and molecule size, we perform structural investigations for 240-atom Si and 120-atom ZrCu, SiO_2, HfO_2, and Al_2O_3 amorphous systems, generating 10 independent structures for each material.

A. Structural investigations

We begin by discussing Si in more detail. An example of the full process from randomly placed molecules in a box to the final amorphous configuration is shown in Fig. 1. The calculated density for Si is 2.25 g/cm^3, which is within the expected experimental range of 2.24 to 2.29 g/cm^3 [45,54,55]. The variation in the experimental densities arises from the difficulty in controlling the pore size and distribution depending on the manufacturing technique [54]. A comparison of calculated and experimental densities for our other case studies is shown in Table II. All of our results are in close agreement with experimental values.

Radial distribution functions (RDFs) are one of the most useful methods for characterizing local atomic distributions in amorphous materials, both theoretically and experimentally, and they provide a more demanding test of our computed amorphous structures than the density alone. The RDF curves for the materials investigated here are plotted and compared with experimental data (as well as the melt-quench method for Si, HfO_2, and ZrCu) in Fig. 4. Peak locations are summarized in Table II. Good agreement is seen in all cases, supporting the accuracy of the MRAS method. We also note that our computed RDF curve and first peak location for Si, one of the most well-studied amorphous materials computationally, are in good agreement with other experimental and computational results [45,54–56].

We further investigate the structural properties produced by MRAS by considering the angular distribution functions (ADF) summed over all atom types, ring statistics, and coordination analysis. The cutoff distances used for these additional investigations are chosen based on the RDF curve's radial value that corresponds to the minimum $g(r)$ value after the first peak (2.75 Å for Si, 2.15 Å for SiO_2, 2.35 Å for HfO_2, 3.65 Å for ZrCu, and 2.20 Å for Al_2O_3). We concentrate on Si, HfO_2, and ZrCu in the main text in order to compare with melt-quench calculations. MRAS results for SiO_2 and Al_2O_3 are available in the Supplemental Material [66]. Figure 5 displays the ADF curves for Si, HfO_2, and ZrCu. The curves for both MRAS and melt-quench follow very similar patterns for the range of observed angles. The curves also follow trends observed in the literature for Si and HfO_2 [19,55]. The ring statistics are displayed in Fig. 6, and again show very strong agreement across methods and materials.

To provide a more detailed comparison of the melt-quench method with the minimization method, we analyze the density of defects in amorphous Si produced with both methods. Defects in amorphous systems are challenging to identify as compared to their crystalline counterparts due to the lack of long-range ordering, making it difficult to identify typical extended defects such as dislocations, stacking faults, etc. Therefore, we focus on short-ranged defects, and in particular under- and overcoordinated atoms. Like crystalline Si, the idealized continuous random network model for amorphous Si [67] has all silicon fourfold coordinated, so we consider under- and overcoordinated Si to be defects. Figure 7 shows the percent of Si with 2, 3, 5, and 6 neighbors, using both the minimization method and melt-quench with various parameters. The minimization method has similar numbers of undercoordinated Si to melt-quench, with slightly more overcoordinated Si, but overall the results are very similar and comparable to previous observations in other melt-quench simulations in the literature [44,68]. This higher number of overcoordinated atoms could be correlated to the slightly higher excess energy per atom for MRAS compared to melt-quench samples as displayed in Table III. This is

TABLE II. Calculated and experimental values for the final average density and average peaks in radial distribution function curves for selected materials.

Material	Density (g/cm^3)	First peak (Å)	Second peak (Å)	Third peak (Å)
Si MRAS	2.25 ± 0.02	2.35		
Si Expt.	2.28 [44,45]	2.35 [54,56]		
SiO_2 MRAS	2.22 ± 0.07	1.65	2.65	3.03
SiO_2 Expt.	2.20 [59–61]	1.61 [61,62]	2.63 [61,62]	3.1 [61,62]
HfO_2 MRAS	8.22 ± 0.19	2.08	2.8	3.28
HfO_2 Expt.	8.1–8.53 [46,47]	2.05–2.13 [21]	2.80 [20]	3.38 [21]
ZrCu MRAS	7.22 ± 0.01	2.53	2.76	3.16
ZrCu Expt.	7.34, 7.41 [48,49]	2.53 [49]	2.75 [49]	3.15 [49]
Al_2O_3 MRAS	3.04 ± 0.07	1.77	2.63	2.98
Al_2O_3 Expt.	2.5–3.4 [14,58,63–65]	1.76, 1.81 [14,58]	2.60 [58]	3.00 [58]

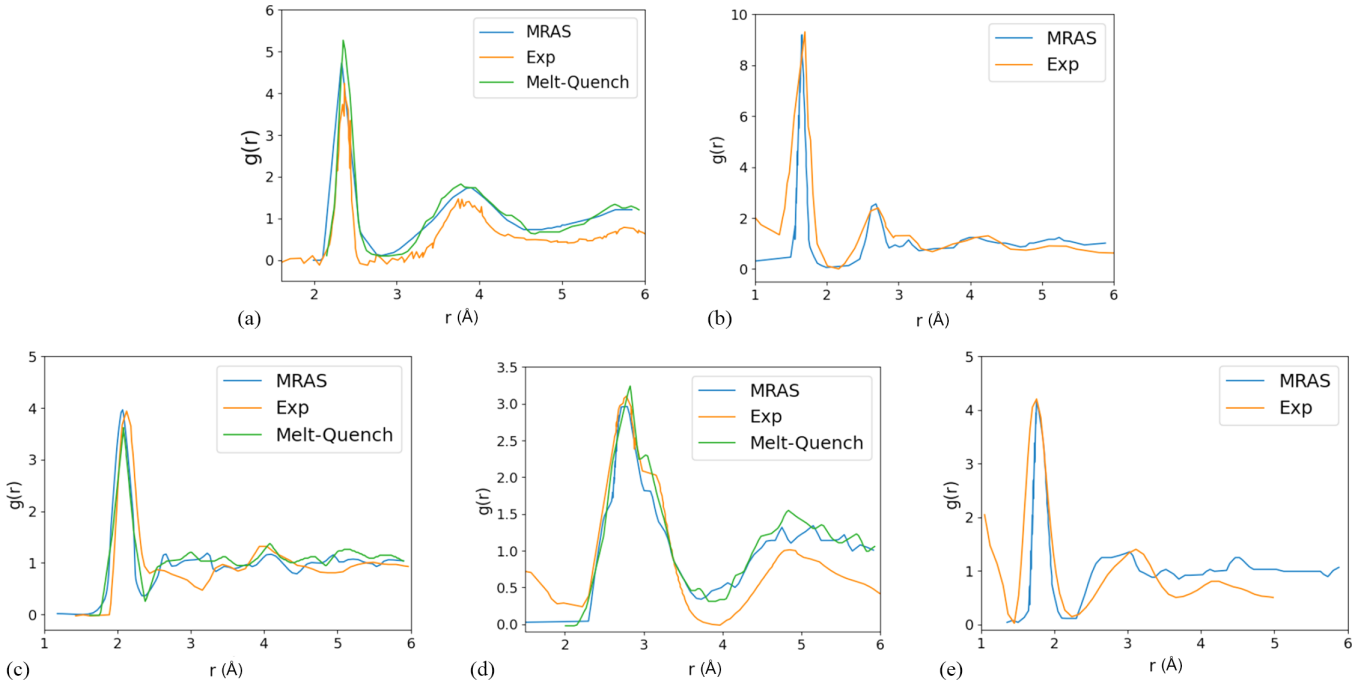

FIG. 4. RDF curves from the minimization method and experimental methods for (a) Si (and melt-quench) [56], (b) SiO_2 [57], (c) HfO_2 (and melt-quench) [21], (d) ZrCu (and melt-quench) [48], and (e) Al_2O_3 [58]. $g(r)$ represents the dimensionless probability of finding a particle at a distance r from another particle, normalized to approach 1 at large distance.

corroborated with other simulation investigations showcasing higher excess energy above diamond silicon for both under- and overcoordinated atoms compared to fourfold-coordinated atoms [68].

While defect analysis is useful for simple amorphous structures like a-Si, more complicated structures like a-HfO_2 and a-ZrCu do not have an easily defined ideal coordination number. However, coordination analysis can still be useful to compare MRAS and melt-quench structures. Figure 8 shows the coordination analysis for the a-HfO_2 and a-ZrCu systems when using MRAS or melt-quench. Additional investigations in the literature also show similar structures produced from larger-scale melt-quench simulations utilizing force fields for amorphous HfO_2 [20].

Thermodynamical internal energies of the amorphous structures produced by MRAS are also compared to those of the corresponding melt-quench structures using molecular dynamics. Each static Si, HfO_2, and ZrCu amorphous structure model was used as the initial structure for an *ab initio* MD run at 300 K. The simulations were run for 10 ps for equilibration followed by 10 ps for the calculation of average internal energy. The ensemble time-averaged energies are displayed in Supplemental Material, Tables S1–S3 along with their standard deviation and uncertainty calculated over 10 ensemble members for MRAS and 5 ensemble members for melt-quench structures. The tables demonstrate that the MRAS/melt-quench internal energy differences in each systems are minimal, less than 0.04 eV per atom in all cases, with MRAS generally but not always showing slightly higher internal energy. The results are also system dependent. For the slowest melt-quenches (20 ps), MRAS internal energies varied from about 0.00 eV per atom higher than melt-quench for ZrCu to about 0.03 eV per atom higher for Si. For the fastest melt-quenches (2 ps), MRAS internal energies were from about 0.02 eV/atom lower than melt-quench for ZrCu to about 0.01 eV/atom higher for HfO_2. These results suggest that overall, MRAS structures are thermodynamically comparable to typical melt-quench structures.

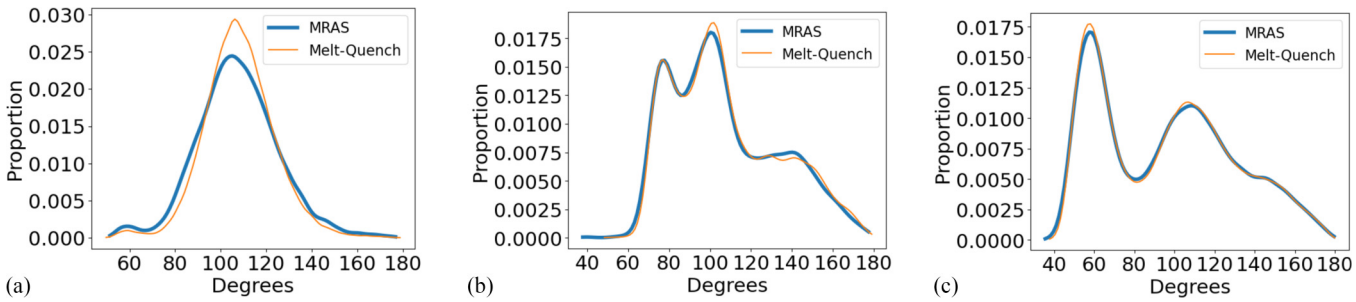

FIG. 5. ADF curves from the minimization method and melt-quench for (a) Si, (b) HfO_2, and (c) ZrCu.

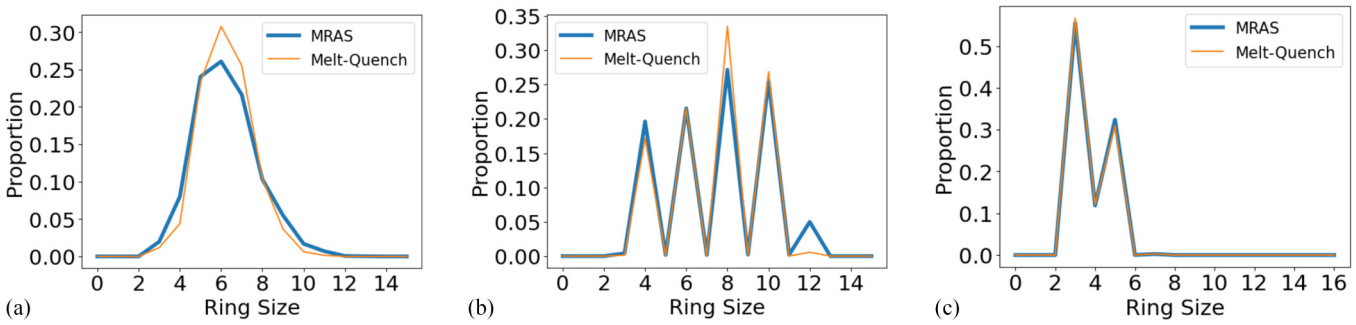

FIG. 6. Ring statistics from the minimization method and melt-quench for (a) Si, (b) HfO_2, and (c) ZrCu.

IV. DISCUSSION

Our above results show that despite the simplicity of MRAS, it can produce accurate structures for amorphous metallic alloys, insulators, and semiconductors. We show that in each case the method is in good agreement with experiment and, for each system that we tested, in good agreement with the melt-quench method as well. The fact that the random initial structures investigated in this paper do not relax into known crystalline structures shows that there are significant barriers preventing our starting configurations from reaching the lowest-energy crystalline structures. This is likely due to the large number of local minima configurations that are possible in materials that form amorphous structures. Our results may appear to be in tension with the successes of the *ab initio* random structure search method, which also relaxes random structures, but with a goal of discovering global minimum configurations [69]. However, we note that we start with large-volume unit cells with over one hundred atoms, and from investigations by Pickard *et al.*, it is highly unlikely for such an initial random structure to minimize into a stable crystalline structure without additional biasing techniques, such as imposing symmetry constraints or perturbing a final structure that could push it towards a lower-energy structure [69]. Similar concepts could be applied to MRAS to bias the final structure towards lower-energy configurations, possibly with additional annealing and relaxation steps that could reduce the excess energy found in our structures compared to melt-quench (Table III) and reduce under- and

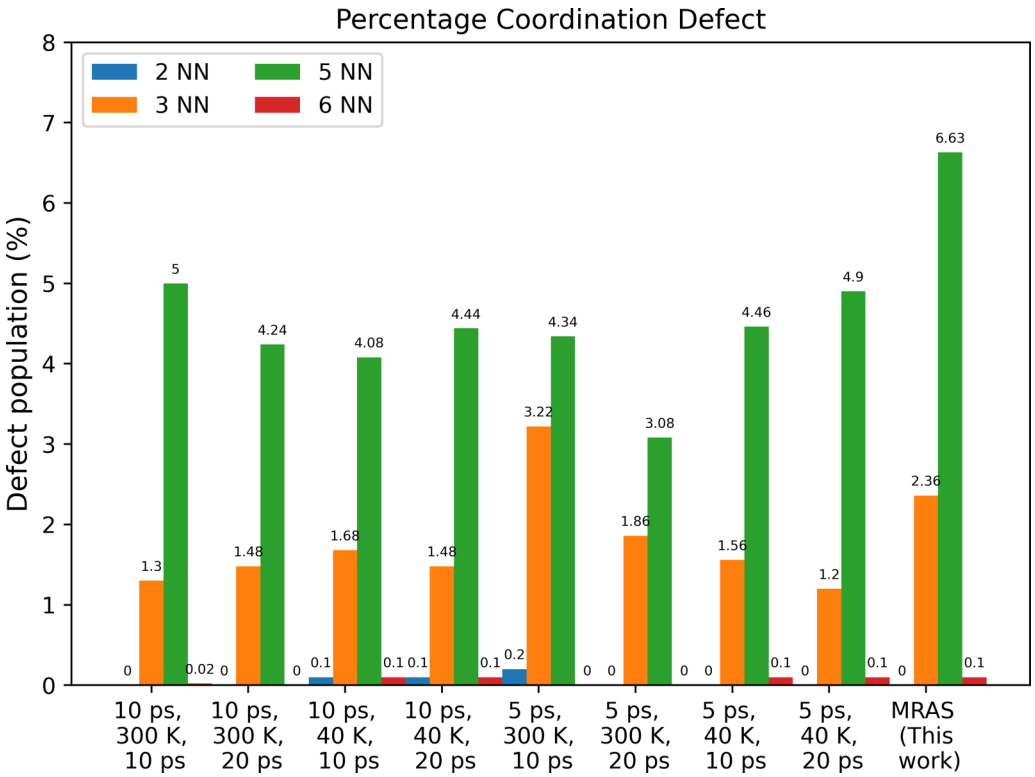

FIG. 7. Percentage of coordination defects in amorphous Si models vs construction method (melt-quench or minimization). The labeling represents the melt-quench melting time, the final temperature, and the quench time. The defects are classified as undercoordinated [2 or 3 nearest neighbors (NN)] or overcoordinated (5 or 6 NN) atoms. The cutoff distance for determining NN is 2.7Å. Melt-quench results are averaged over 5 runs each, minimization method over 10 relaxations.

TABLE III. Average energy per atom of amorphous silicon for MRAS and melt-quench simulations.

System	Excess energy per atom (eV)
MRAS	0.306
10-ps melt, 300 K, 10-ps quench	0.281
10-ps melt, 300 K, 20-ps quench	0.267
10-ps melt, 40 K, 10-ps quench	0.262
10-ps melt, 40 K, 20-ps quench	0.252
5-ps melt, 300 K, 10-ps quench	0.281
5-ps melt, 300 K, 20-ps quench	0.282
5-ps melt, 40 K, 10-ps quench	0.263
5-ps melt, 40 K, 20-ps quench	0.262

overcoordinated atoms. Alternately, it would be interesting to explore nonrandom initial molecular arrangements that *do* relax directly to a crystal.

Consistent with our goals, we find that MRAS is less computationally expensive than melt-quench. We compared the performance of MRAS with that of the quickest melt-quench conducted in this paper: 5-ps melt, 10-ps quench time to 300 K, and a 5-ps target temperature hold. The VASP input parameters for each method were as similar as possible except that the stress tensor was not calculated for the melt-quench runs. We ran MRAS three times while we ran the melt-quench once (since computational resources should be similar between different simulation runs) on the same hardware with different random numerical seeds. The average number of core hours for the MRAS is 24 h while melt-quench is 116 h (see Table IV for details). This is significant as one of the main bottlenecks for theoretically examining amorphous structures is the large computational burden. It may be possible to further optimize the computational cost of our method by choosing smaller initial volumes and separation distances, while maintaining agreement with experimental densities. For example, Fig. 3 suggests that 5× the expected bulk crystalline volume with roughly 1.2× molecule length could be used as an initial configuration to produce similar densities at even lower computational costs, but further investigations are necessary to verify the efficiency of using alternative choices of parameters. Additionally, the only material-specific input parameters that our method requires are the lengths of the individual molecules and the approximate density of the base crystalline material. The density plus minimum separation distance heuristic reported here reproduces the experimental amorphous density of all the systems investigated well, despite the lack of theoretical justification for these values. A more rigorous justification of this aspect would enhance the value of MRAS over typical fixed-volume melt-quench techniques that require a prior understanding of the density of the amorphous material and the melting temperature to obtain a simulation cell consistent with this density. This is an issue for amorphous structures with densities that differ significantly from their crystalline counterparts. For example, the experimental amorphous Al_2O_3 density is found to be between 2.5 and 3.4 g/cm^3 [14,58,63–65] compared to the

TABLE IV. Computational resources and computation time for MRAS and melt-quench simulations.

Method	CPU	RAM	Cores	Core hours
MRAS	Epyc 7702	512 GB	64	24
Melt-quench	Epyc 7702	512 GB	64	116

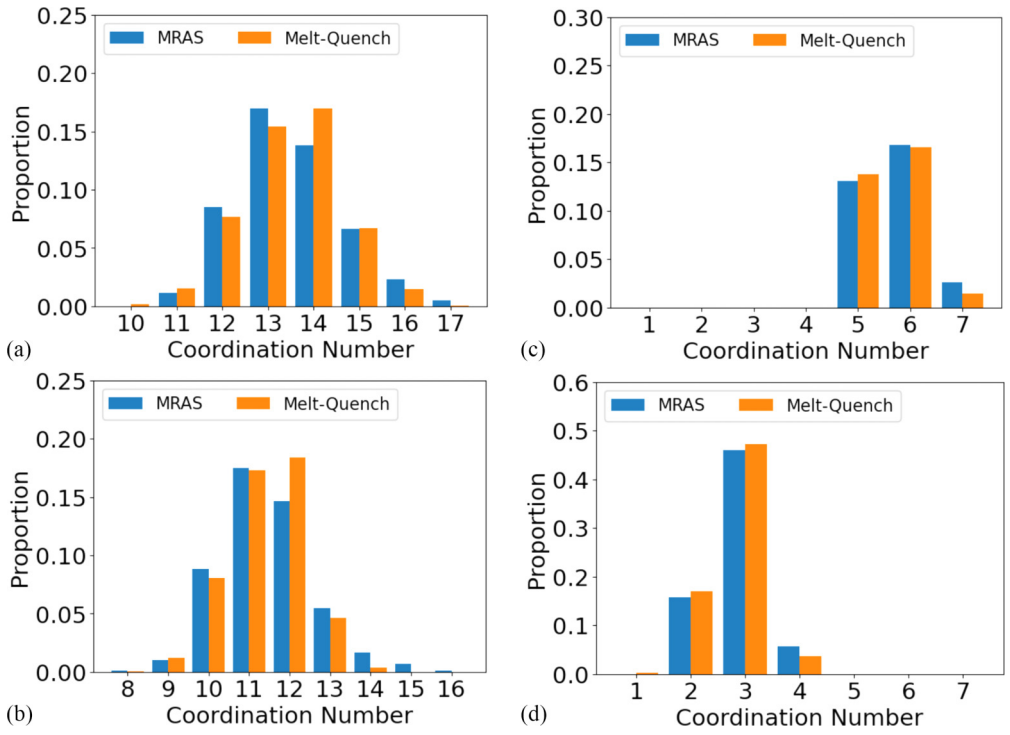

FIG. 8. Coordination analysis from the minimization method and melt-quench for HfO_2 [Hf (a) and O (b)] and ZrCu [Zr (c) and Cu (d)].

crystalline α-Al (corundum) phase, which is 3.95 g/cm^3 [70]. Without prior knowledge of the amorphous density, obtaining appropriate amorphous structures through melt-quench would require a method to guess or optimize the density. One geometric packing model suggests a density reduction between 10 and 15% for organic and inorganic amorphous solids compared to their crystalline counterparts [71], but even this model works poorly for Al_2O_3. It would suggest an Al_2O_3 amorphous density range of 3.36 to 3.56 g/cm^3, which is larger than many of the experimentally observed samples, whereas the MRAS value of 3.05 g/cm^3 is closer to the middle of the experimental densities. The ability to readily obtain accurate amorphous densities with MRAS as compared to melt-quench methods and the fact that no known parent amorphous structure is required for MRAS make this method potentially useful for constructing amorphous structure models in more complex systems.

V. CONCLUSIONS

We propose molecule relaxation for amorphous structures (MRAS) as a method for modeling amorphous structures solely using structural relaxation methods. We demonstrate that the method has lower computational cost than the melt-quench technique with similar accuracy. MRAS is based on a heuristic used to generate initial structures that we show leads to good agreement between simulated and experimental amorphous structures across a variety of systems, even in the case of Al_2O_3, where the amorphous density is significantly lower than that of the crystalline corundum phase. Additionally, the reduced computational cost allows for a larger quantity of structures to be produced, which may be useful in generating training data for machine learning of amorphous systems. We expect our minimization method to facilitate an accelerated understanding of the amorphous structures that span a wide swath of the material space.

ACKNOWLEDGMENTS

This work was performed with funding from the CHIPS Metrology Program, part of CHIPS for America, National Institute of Standards and Technology, U.S. Department of Commerce.

Certain commercial software packages are mentioned in this paper in order to specify the procedures used and to display the results. It does not imply recommendation or endorsement by NIST nor does it imply that the software packages identified are necessarily the best available for the purpose.

There are no conflicts of interest.

DATA AVAILABILITY

Visual displays of atomic systems were created using the OVITO software [72]. The code is available at the GitHub repository [73]. Data on initial and final structures and DFT input parameters used are deposited in the NIST Data Publication [74].

[1] T. Kamiya and H. Hosono, Material characteristics and applications of transparent amorphous oxide semiconductors, NPG Asia Mater. **2**, 15 (2010).

[2] *Amorphous Oxide Semiconductors: IGZO and Related Materials for Display and Memory*, 1st ed., edited by H. Hosono and H. Kumomi (Wiley, 2022).

[3] J. Mort, Applications of amorphous materials, Phys. Technol. **11**, 134 (1980).

[4] S. Saraswat, V. K. Tomar, V. K. Deolia, and N. Mehta, A brief review of amorphous semiconductors, Mater. Today: Proceedings (2023), doi:10.1016/j.matpr.2023.03.455.

[5] A. M. Stoneham, J. L. Gavartin, and A. L. Shluger, The oxide gate dielectric: Do we know all we should? J. Phys.: Condens. Matter **17**, S2027 (2005).

[6] J. K. Christie, Review: Understanding the properties of amorphous materials with high-performance computing methods, Philos. Trans. R. Soc. A **381**, 20220251 (2023).

[7] A. Tilocca, Cooling rate and size effects on the medium-range structure of multicomponent oxide glasses simulated by molecular dynamics, J. Chem. Phys. **139**, 114501 (2013).

[8] V. B. Sulimov, D. C. Kutov, A. V. Sulimov, F. V. Grigoriev, and A. V. Tikhonravov, Density functional modeling of structural and electronic properties of amorphous high temperature oxides, J. Non-Cryst. Solids **578**, 121170 (2022).

[9] A. F. Harper, S. P. Emge, P. C. M. M. Magusin, C. P. Grey, and A. J. Morris, Modelling amorphous materials via a joint solid-state NMR and X-ray absorption spectroscopy and DFT approach: Application to alumina, Chem. Sci. **14**, 1155 (2023).

[10] V. L. Deringer, N. Bernstein, A. P. Bartók, M. J. Cliffe, R. N. Kerber, L. E. Marbella, C. P. Grey, S. R. Elliott, and G. Csányi, Realistic atomistic structure of amorphous silicon from machine-learning-driven molecular dynamics, J. Phys. Chem. Lett. **9**, 2879 (2018).

[11] H. Zheng, E. Sivonxay, M. Gallant, Z. Luo, M. McDermott, P. Huck, and K. A. Persson, The *ab initio* amorphous materials database: Empowering machine learning to decode diffusivity, arXiv:2402.00177.

[12] J. P. Trinastic, R. Hamdan, Y. Wu, L. Zhang, and H.-P. Cheng, Unified interatomic potential and energy barrier distributions for amorphous oxides, J. Chem. Phys. **139**, 154506 (2013).

[13] G. Gutiérrez and B. Johansson, Molecular dynamics study of structural properties of amorphous Al_2O_3, Phys. Rev. B **65**, 104202 (2002).

[14] H. Hashimoto *et al.*, Structure of alumina glass, Sci. Rep. **12**, 516 (2022).

[15] W. L. Scopel, A. J. R. da Silva, and A. Fazzio, Amorphous HfO_2 and $Hf_{1-x}Si_xO$ via a melt-and-quench scheme using *ab initio* molecular dynamics, Phys. Rev. B **77**, 172101 (2008).

[16] G. H. Chen, Z. F. Hou, and X. G. Gong, Density functional calculations on atomic and electronic structures of amorphous HfO_2/Si(001) interface, Appl. Phys. Lett. **95**, 102905 (2009).

[17] T.-J. Chen and C.-L. Kuo, First principles study of the structural, electronic, and dielectric properties of amorphous HfO_2, J. Appl. Phys. **110**, 064105 (2011).

[18] G. Broglia, G. Ori, L. Larcher, and M. Montorsi, Molecular dynamics simulation of amorphous HfO_2 for resistive RAM applications, Modell. Simul. Mater. Sci. Eng. **22**, 065006 (2014).

[19] T. H. Nguyen, V. V. Le, and T. N. Nguyen, Molecular dynamics simulation of structural properties in amorphous HfO_2 under cooling process, Vacuum **161**, 251 (2019).

[20] Y. Wang, F. Zahid, J. Wang, and H. Guo, Structure and dielectric properties of amorphous high-k oxides: HfO_2, ZrO_2, and their alloys, Phys. Rev. B **85**, 224110 (2012).

[21] L. C. Gallington *et al.*, The structure of liquid and amorphous hafnia, Materials **10**, 1290 (2017).

[22] C. Ben Mahmoud, A. Anelli, G. Csányi, and M. Ceriotti, Learning the electronic density of states in condensed matter, Phys. Rev. B **102**, 235130 (2020).

[23] N. Castel and F.-X. Coudert, Challenges in molecular dynamics of amorphous ZIFs using reactive force fields, J. Phys. Chem. C **126**, 19532 (2022).

[24] A. Madanchi *et al.*, Is the future of materials amorphous? Challenges and opportunities in simulations of amorphous materials, ACS Phys. Chem. Au **5**, 3 (2025).

[25] R. Strickstrock, M. Hülsmann, D. Reith, and K. N. Kirschner, Optimizing Lennard-Jones parameters by coupling single molecule and ensemble target data, Comput. Phys. Commun. **274**, 108285 (2022).

[26] X. Hao, J. Liu, M. Deng, and Z. Fan, Critical evaluation of five classical force fields for $CsPbI_3$: Limitations in modeling phase stability and transformations, J. Phys. Chem. C **127**, 20157 (2023).

[27] D. E. Carlson and C. R. Wronski, Amorphous silicon solar cell, Appl. Phys. Lett. **28**, 671 (1976).

[28] M. Shibata, Y. Sakai, and D. Yokoyama, Advantages and disadvantages of vacuum-deposited and spin-coated amorphous organic semiconductor films for organic light-emitting diodes, J. Mater. Chem. C **3**, 11178 (2015).

[29] E. Gusev, C. Cabral, M. Copel, C. D'Emic, and M. Gribelyuk, Ultrathin HfO_2 films grown on silicon by atomic layer deposition for advanced gate dielectrics applications, Microelectron. Eng. **69**, 145 (2003).

[30] J. Arvo, Fast random rotation matrices, in *Graphics Gems III (IBM Version)* (Elsevier, 1992), pp. 117–120.

[31] N. F. Quackenbush, E. Cockayne, J. M. Ablett, D. P. Siddons, J. C. Woicik, and A. K. Rumaiz, Accurate band alignment at the amorphous Al_2O_3/p-Ge(100) interface determined by hard x-ray photoelectron spectroscopy and density functional theory, Phys. Rev. Mater. **2**, 114605 (2018).

[32] J. A. W. Harkless, D. K. Stillinger, and F. H. Stillinger, Structures and energies of SiO_2 clusters, J. Phys. Chem. **100**, 1098 (1996).

[33] S. Li and D. A. Dixon, Molecular structures and energetics of the $(ZrO_2)_n$ and $(HfO_2)_n (n = 1–4)$ clusters and their anions, J. Phys. Chem. A **114**, 2665 (2010).

[34] A. B. Rahane, M. D. Deshpande, and V. Kumar, Structural and electronic properties of $(Al_2O_3)_n$ clusters with $n = 1–10$ from first principles calculations, J. Phys. Chem. C **115**, 18111 (2011).

[35] N. Binggeli, J. L. Martins, and J. R. Chelikowsky, Simulation of Si clusters via Langevin molecular dynamics with quantum forces, Phys. Rev. Lett. **68**, 2956 (1992).

[36] W. Kohn and L. J. Sham, Self-consistent equations including exchange and correlation effects, Phys. Rev. **140**, A1133 (1965).

[37] G. Kresse and J. Hafner, *Ab initio* molecular dynamics for liquid metals, Phys. Rev. B **47**, 558 (1993).

[38] G. Kresse and J. Furthmüller, Efficiency of ab-initio total energy calculations for metals and semiconductors using a plane-wave basis set, Comput. Mater. Sci. **6**, 15 (1996).

[39] G. Kresse and J. Furthmüller, Efficient iterative schemes for ab initio total-energy calculations using a plane-wave basis set, Phys. Rev. B **54**, 11169 (1996).

[40] J. Hafner and G. Kresse, in *Properties of Complex Inorganic Solids*, edited by A. Gonis, A. Meike, and P. E. A. Turchi (Springer US, Boston, MA, 1997), pp. 69–82.

[41] G. Kresse and D. Joubert, From ultrasoft pseudopotentials to the projector augmented-wave method, Phys. Rev. B **59**, 1758 (1999).

[42] P. E. Blöchl, Projector augmented-wave method, Phys. Rev. B **50**, 17953 (1994).

[43] J. P. Perdew, K. Burke, and M. Ernzerhof, Generalized gradient approximation made simple, Phys. Rev. Lett. **77**, 3865 (1996).

[44] W. Li and Y. Ando, Dependence of a cooling rate on structural and vibrational properties of amorphous silicon: A neural network potential-based molecular dynamics study, J. Chem. Phys. **151**, 114101 (2019).

[45] K. Laaziri, S. Kycia, S. Roorda, M. Chicoine, J. L. Robertson, J. Wang, and S. C. Moss, High-energy X-ray diffraction study of pure amorphous silicon, Phys. Rev. B **60**, 13520 (1999).

[46] S. Jena *et al.*, Influence of oxygen partial pressure on microstructure, optical properties, residual stress and laser induced damage threshold of amorphous HfO_2 thin films, J. Alloys Compd. **771**, 373 (2019).

[47] K.-M. Kim, J. S. Jang, S.-G. Yoon, J.-Y. Yun, and N.-K. Chung, Structural, optical and electrical properties of HfO_2 thin films deposited at low-temperature using plasma-enhanced atomic layer deposition, Materials **13**, 2008 (2020).

[48] X. Wu *et al.*, Multiscale structures of Zr-based binary metallic glasses and the correlation with glass forming ability, Prog. Nat. Sci.: Mater. Int. **27**, 482 (2017).

[49] H. S. Chen and Y. Waseda, Structure of glassy ZrCu and NbNi alloys, Phys. Status Solidi A **51**, 593 (1979).

[50] E. P. Donovan, F. Spaepen, D. Turnbull, J. M. Poate, and D. C. Jacobson, Heat of crystallization and melting point of amorphous silicon, Appl. Phys. Lett. **42**, 698 (1983).

[51] B. Johnson and J. L. Jones, in *Ferroelectricity in Doped Hafnium Oxide: Materials, Properties and Devices* (Elsevier, 2019), pp. 25–45.

[52] E. M. Carvalho and I. R. Harris, Constitutional and structural studies of the intermetallic phase, ZrCu, J. Mater. Sci. **15**, 1224 (1980).

[53] J. Qiao *et al.*, Structural heterogeneities and mechanical behavior of amorphous alloys, Prog. Mater. Sci. **104**, 250 (2019).

[54] J. Fortner and J. S. Lannin, Radial distribution functions of amorphous silicon, Phys. Rev. B **39**, 5527 (1989).

[55] A. Pedersen, L. Pizzagalli, and H. Jónsson, Optimal atomic structure of amorphous silicon obtained from density functional theory calculations, New J. Phys. **19**, 063018 (2017).

[56] K. Laaziri, S. Kycia, S. Roorda, M. Chicoine, J. L. Robertson, J. Wang, and S. C. Moss, High resolution radial distribution function of pure amorphous silicon, Phys. Rev. Lett. **82**, 3460 (1999).

[57] H. Ohsaki and M. Tada, High energy electron diffraction study on ionic character of amorphous SiO_2, Jpn. J. Appl. Phys. **25**, 1768 (1986).

[58] A. Pugliese *et al.*, Atomic-layer-deposited aluminum oxide thin films probed with x-ray scattering and compared to molecular dynamics and density functional theory models, ACS Omega **7**, 41033 (2022).

[59] S. Kohara *et al.*, Relationship between diffraction peak, network topology, and amorphous-forming ability in silicon and silica, Sci. Rep. **11**, 22180 (2021).

[60] H. Masai *et al.*, Siliceous zeolite-derived topology of amorphous silica, Commun. Chem. **6**, 269 (2023).

[61] H. Morikawa, S.-I. Miwa, M. Miyake, F. Marumo, and T. Sata, Structural analysis of SiO_2–Al_2O_3 glasses, J. Am. Ceram. Soc. **65**, 78 (1982).

[62] D. A. Keen and M. T. Dove, Local structures of amorphous and crystalline phases of silica, SiO_2, by neutron total scattering, J. Phys.: Condens. Matter **11**, 9263 (1999).

[63] A. H. Tavakoli *et al.*, Amorphous alumina nanoparticles: Structure, surface energy, and thermodynamic phase stability, J. Phys. Chem. C **117**, 17123 (2013).

[64] S. P. Adiga, P. Zapol, and L. A. Curtiss, Atomistic simulations of amorphous alumina surfaces, Phys. Rev. B **74**, 064204 (2006).

[65] H. Momida, T. Hamada, Y. Takagi, T. Yamamoto, T. Uda, and T. Ohno, Theoretical study on dielectric response of amorphous alumina, Phys. Rev. B **73**, 054108 (2006).

[66] See Supplemental Material at http://link.aps.org/supplemental/10.1103/8cdr-bk3f for supplemental figures S1 and S2 showcasing angular distribution function and ring statistics for SiO_2 and Al_2O_3. Supplemental tables I–III showcase average internal energy of MRAS and melt-quench amorphous structures of Si, HfO_2, and ZrCu.

[67] Y. Tu, J. Tersoff, G. Grinstein, and D. Vanderbilt, Properties of a continuous-random-network model for amorphous systems, Phys. Rev. Lett. **81**, 4899 (1998).

[68] J. D. Morrow *et al.*, Understanding defects in amorphous silicon with million-atom simulations and machine learning, Angew. Chem. Int. **63**, e202403842 (2024).

[69] C. J. Pickard and R. J. Needs, *Ab initio* random structure searching, J. Phys.: Condens. Matter **23**, 053201 (2011).

[70] L. Aarik, H. Mändar, A. Tarre, H.-M. Piirsoo, and J. Aarik, Mechanical properties of crystalline and amorphous aluminum oxide thin films grown by atomic layer deposition, Surf. Coat. Technol. **438**, 128409 (2022).

[71] X.-Y. Cui, S. P. Ringer, G. Wang, and Z. H. Stachurski, What should the density of amorphous solids be? J. Chem. Phys. **151**, 194506 (2019).

[72] A. Stukowski, Visualization and analysis of atomistic simulation data with OVITO–The open visualization tool, Modell. Simul. Mater. Sci. Eng. **18**, 015012 (2010).

[73] J. Worden, Github, 2025, https://github.com/jawordenNIST/Molecule-Relaxation-for-Amorphous-Structures-MRAS-.git.

[74] J. Worden, E. Cockayne, and K. F. Garrity, Construction of amorphous structure models via relaxation of random arrangements of molecules, dataset, National Institute of Standards and Technology, Version: 1.0 (2025), https://doi.org/10.18434/mds2-3831.